Journal of Colloid and Interface Science 538 (2019) 433–439

Contents lists available at ScienceDirect

Journal of Colloid and Interface Science

journal homepage: www.elsevier.com/locate/jcis

Regular Article

# Carboxylated nanocellulose foams as superabsorbents

Llyza Mendoza, Laila Hossain, Emma Downey, Camilla Scales, Warren Batchelor, Gil Garnier *

*Bioresource Processing Research Institute of Australia (BioPRIA), Department of Chemical Engineering, Monash University, VIC 3800, Australia*

## GRAPHICAL ABSTRACT

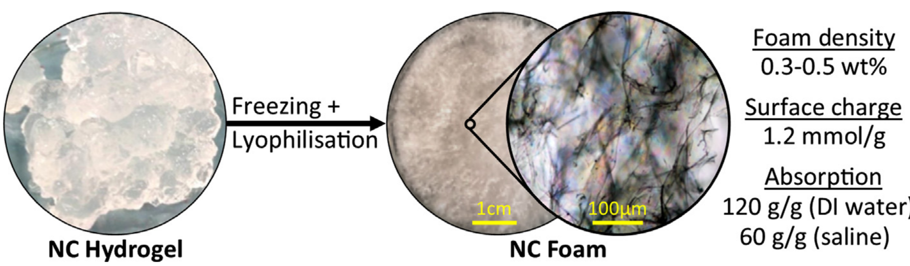


## ARTICLE INFO

*Article history:*
Received 25 October 2018
Revised 29 November 2018
Accepted 30 November 2018
Available online 1 December 2018

*Keywords:*
Superabsorbent
TEMPO-mediated oxidation
Nanocellulose
Foam
Structure

## ABSTRACT

*Hypothesis:* Carboxylated nanocellulose fibres formed into foam structures can demonstrate superabsorption capacity. Their performance can be engineered by changing process variables.
*Experiments:* TEMPO-oxidised cellulose nanofibres of varying concentration and surface charge are produced from hardwood kraft pulp. Foams were prepared through a 2-step freezing and lyophilisation process. The absorption capacity of water and saline solution (0.9 wt%) were measured as a function of time and related to the foam structure.
*Findings:* The absorption capacity of nanocellulose foams can be manipulated from initial gel properties and processing conditions. Pore structure and distribution of nanocellulose foams are dictated by fibre content and charge density and freezing rate. The best performing foams are at 0.3–0.5 wt%, with a carboxylate concentration of 1.2 mmol/g and frozen at −86 °C before freeze-drying, which can absorb 120 g $H_2O$/g fibre. Fibre surface charge influences the absorption capacity of the foams by dictating the amount of participating carboxylate groups. Absorption capacity in saline (60 g/g) is lower than in deionised water (120 g/g); but is only slightly lower than that of a commercial polyacrylic acid (PAA) SAPs (80 g/g). Nanocellulose foams are attractive renewable alternatives for superabsorbent applications, contributing to a reduction of plastic microspheres.


## 1. Introduction

Superabsorbent polymer (SAP) hydrogels contain cross-linked network of hydrophilic polymers capable of absorbing large volumes of water [1]. Upon contact with water, the glassy polymers hydrate to form a three-dimensional network which does not dissolve due to the presence of cross-linking [2]. The swelling of these polymer networks is driven by the difference in osmotic pressure inside and outside the gel caused by the movement of the counterions in the system. The high absorption of water molecules is due to a high concentration of $COO^-$ groups able to form hydrogen bonding with water molecules [3]. Although commercial SAPs are usually known for applications in personal care and hygiene products, these materials are also increasingly utilised in agriculture and horticulture [4], biomedical products [5–7], and even wastewater treatment [8,9]. Currently, the majority of superabsorbent products in the market is synthesised from acrylic and acrylamide

* Corresponding author.
*E-mail address:* gil.garnier@monash.edu (G. Garnier).

https://doi.org/10.1016/j.jcis.2018.11.112

polymers from petrochemicals which exhibit poor environmental degradability. This lack of sustainability has driven research towards developing alternatives which are renewably sourced and biodegradable.

There are many reports of superabsorbents made from natural polymers in literature. Natural-based SAPs, such as chitosan, gelatine, carrageenan and starch, have been modified to increase water absorption [10,11]. Cellulose, the most abundant biopolymer, has also been studied for its desirable characteristics: biodegradability, renewability, and innate hydrophilicity [12]. Cellulose can be processed into porous materials such as foams [13,14] and different synthesis methods have been explored to functionalise cellulose as a superabsorbent hydrogel [12]. Among those are foam and hydrogel composites made with carboxymethyl cellulose [15–19] and hydroxyethyl cellulose [20,21] used in combination with other polymers and nanoparticles. Another strategy is to graft side groups such as butanetetracarboxyl, acrylic, and acrylamide groups onto the cellulose backbone which results in large absorption of water (~720 g/g) [22,23]. Functionalising the cellulose hydroxyl groups can significantly increase water interactions.

Another method of producing foams is through the production of nanocellulose and manufacture of foams via ice-templating followed by sublimation or via supercritical drying [24]. TEMPO-mediated oxidation is alternative method of functionalising cellulose fibres [25]. This oxidation process selectively converts the primary alcohol (C6) groups into carboxylate groups. The added electrostatic repulsion produces nano-scale fibres upon mechanical fibrillation. Brodin and Theliander initially tested the superabsorbent characteristics of TEMPO-oxidised nanocellulose by varying different process conditions such as pulp types, composition, and oxidation severity [26–29]. Jiang and Hsieh investigated the production of nanocellulose aerogels via cyclic freeze-thawing process and also introduced functionalisation to create oleophilic foams [30–32]. However, the effects of varying foam properties by changing the fibre density were not explored nor related to composite structure. There are limited studies on the effect of processing conditions (i.e. freezing rate) on the performance of nanocellulose foams. Moreover, the kinetics of nanocellulose foam swelling remain unknown.

In this study, we produced nanocellulose superabsorbent foams via a two-step process: (1) TEMPO-mediated oxidation/high-pressure homogenisation to produce a nanocellulose hydrogel [33,34] and (2) freeze-drying the hydrogel to produce nanocellulose foams. The aim of this study is to understand the relationship between process variables (freezing rate) and nanocellulose properties (surface charge and fibre concentration) to the resulting foam structure and absorption characteristics. The swelling kinetics of the foams is also determined. Insight into the mechanism of superabsorbency of these carboxylated nanocellulose foams is demonstrated.

## 2. Methodology

### 2.1. Materials

Bleached Eucalyptus Kraft (BEK) pulp, containing approximately 10 wt% solids, was obtained from Australian Paper, Maryvale, Australia. 2,2,6,6-Tetramethylpiperidine-1-oxyl (TEMPO) and sodium bromide (NaBr) were purchased from Sigma-Aldrich. Hydrochloric acid (HCl) and Sodium Hydroxide (NaOH) were diluted for solutions as required and were purchased from ACL Laboratories and Merck, respectively. 12 w/v% Sodium Hypochlorite (NaClO) was purchased from Thermo Fisher Scientific and used as received. Commercial sodium polyacrylate superabsorbent (HySORB R 8130) was provided by BASF.

### 2.2. TEMPO-mediated oxidation

The TEMPO-mediated oxidation process employed is based on a previously developed method [25]. 100 g BEK pulp was suspended in 2500 mL water containing 0.4 g TEMPO and 2.5 g NaBr. The 12 w/v% NaClO solution was initially adjusted to pH 10 via addition of 36 w/v% HCl. To produce high surface charged fibres, 75 mL NaClO (5 mmol NaClO/g cellulose) was added drop-wise to the suspension whilst stirred. Lower surface charged fibres were produced by adding a lower amount of the primary oxidant (50 mL NaClO, 3.33 mmol/g). The pH of the reaction was maintained at 10 through the addition of 0.5 M NaOH. The oxidation process is deemed to be complete when the pH change is negligible. The oxidised fibres were recovered through filtration and stored refrigerated (2–8 °C).

The TEMPO-oxidised pulp is then dispersed in deionised water at a desired concentration. Fibrillation is accomplished through a high-pressure homogeniser (GEA Niro Soavi Homogeniser Panda) at 1000 bar. Suspensions which contain less than 1 wt% TEMPO-oxidised pulp is homogenised with two passes. More concentrated suspensions are homogenised with only one pass.

### 2.3. Preparation of nanocellulose foams

Nanocellulose foams were prepared by spreading 15 g gel in a 50 mm petri dish and freezing at either in a freezer for at least 12 h (−20 °C, −80 °C) or in liquid nitrogen (−196 °C). For freezing at −196 °C, the samples were placed in a cold-proof container and liquid nitrogen was poured in ensuring full immersion for 4–5 min. Once frozen, all samples were freeze-dried (Christ Alpha 2–4 LD Plus) for 2 days.

### 2.4. Determining solids concentration

The solids concentration of any sample (i.e. hydrogel or pulp) is determined through oven drying. The sample is weighed before ($w_i$) and after ($w_d$) drying, where the sample moisture is evaporated in a ventilated oven at 105 °C for at least 4 h. The solids content is determined through the following equation:

$$Solids\ content\ (\%) = \frac{w_d}{w_i} \times 100\% \quad (1)$$

### 2.5. Determining the carboxylate content of nanocellulose

The carboxylate content of the nanocellulose fibre is determined via conductometric titration [35]. 0.1 dry g oxidised pulp is suspended in 40 mL deionised water. 100 μL 1 wt% NaCl is added to the suspension to increase base sample conductivity. The sample pH is then lowered to pH 2.5–3 to protonate all of the carboxylate groups prior to the beginning of titration. Sample titration is initiated by the addition of 0.1 mL/min NaOH (Mettler Toledo T5 titrator). The conductivity is monitored throughout the progress of the titration. The amount of carboxylate groups is then calculated through the following equation:

$$Carboxylate\ Content\ \left(\frac{mmol}{g}\right) = \frac{c(V_2 - V_1)}{w} x100 \quad (2)$$

where $V_2$ and $V_1$ pertain to the required amount of titrant to neutralise the carboxylic groups (plateau region in the titration curve), $c$ is the NaOH concentration (mol/L), and $w$ is the dray sample weight.

### 2.6. Measurement of absorption capacity

The freeze-dried fibres are then allowed to be in contact with deionised water or 0.9 wt% NaCl solution for reabsorption. The foams were repeatedly taken out of immersion and weighed.

Intake of water by the foam is measured in regular intervals up to 2 h. The free swell capacity $W$ is then calculated through the following equation:

$$Free\ Swell\ Capacity,\ W = \frac{m_t - m_i}{m_i} \quad (3)$$

where $m_t$ is the mass of the swollen foam at a particular time interval and $m_i$ is the initial mass of the foam. The results are reported as the average and standard deviation of 3 replicates.

### *2.7. Imaging of nanocellulose structure*

Nanocellulose foams were imaged by optical microscopy (Nikon Eclipse Ni-E Upright Microscope) in bright-field mode at 5x magnification.

### *2.8. Mercury porosimetry*

The pore size distribution, porosity (total and at P = 1 atm), and pore surface area were determined for selected nanocellulose foams via mercury porosimetry (Micromeritics Autopore IV). Nanocellulose foams were cut in small cubes (0.5 × 0.5 × 0.5 cm) by a laser cutter (Epilog Laser Helix). The samples were prepared by initially de-gassing (24 h, 100 °C) followed by testing. Two replicates per sample were tested. In all measurements, the contact angle at the Hg-Foam interface is assumed to be 130° and a testing pressure range from 0.1 to 60,000 psia is applied. The desired values are calculated via the Washburn Equation:

$$D = \frac{-4\gamma \cos\theta}{P} \quad (4)$$

where $D$ is the pore diameter, $\gamma$ is the surface tension of mercury, $\theta$ is the contact angle between the pore wall and mercury, and P is the applied pressure. Important values are reported at either as a result of considering 1 atm (14.7 psia) intrusion pressure or at total maximum porosimetry pressure (60,000 psia/4082 atm).

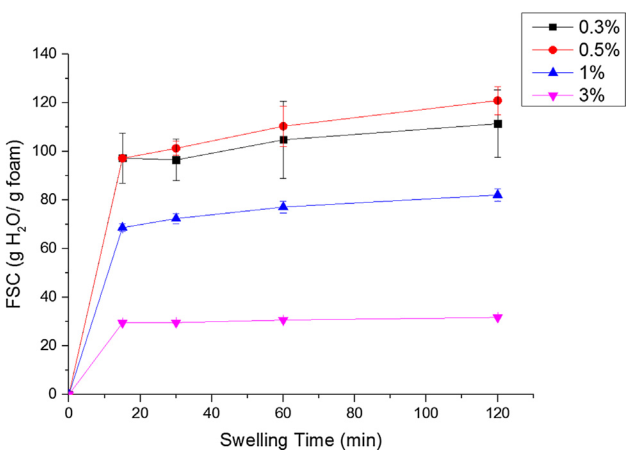


**Fig. 1.** Free Swell Capacity (FSC) in deionised water of nanocellulose foams (−80 °C) at different solids concentrations as a function of swelling time.

## 3. Results

The effect of initial gel properties such as the solids concentration and surface charge on the structure and morphology as well as the absorption behaviour of the foams is initially studied (frozen at -80 °C). The effect of freezing rate is then analysed. Lastly, the best performing foam in distilled water is tested with saline and compared against a commercial SAP.

### *3.1. Effect of gel solids concentration*

Fig. 1 shows the free swell capacity (FSC) of nanocellulose foams in deionised water as a function of the initial gel solids concentration in deionised water. In all cases, the initial rapid swelling is followed by a slower absorption process in the 2 h testing period. There is no significant difference between the performance of foams produced from 0.3 wt% and 0.5 wt% (overlapping error bars). Measurement error also increases at lower initial gel concentrations. However, increasing the fibre concentration in gel from 0.5 wt% to 1 and 3 wt% resulted in a decrease in the FSC values.

The pore size distribution of nanocellulose foams was measured by mercury porosimetry as a function of the initial gel solids concentration is shown in Fig. 2A. Calculated foam properties for each of the nanocellulose foams is also summarised in Fig. 2B and C. At increasing initial gel solids concentration, the foam bulk density consistently increases. Foam porosity is calculated at two pressure levels (1 atm and at 4082 atm) to signify pores accessible at atmospheric pressure and the total maximum pore volume, respectively. Total foam porosity is similar (>94%) across all original gel concentrations; however, porosity at 1 atm is halved when the solids content is increased by an order of magnitude. The total pore surface area also decreased with increasing gel solids concentration.

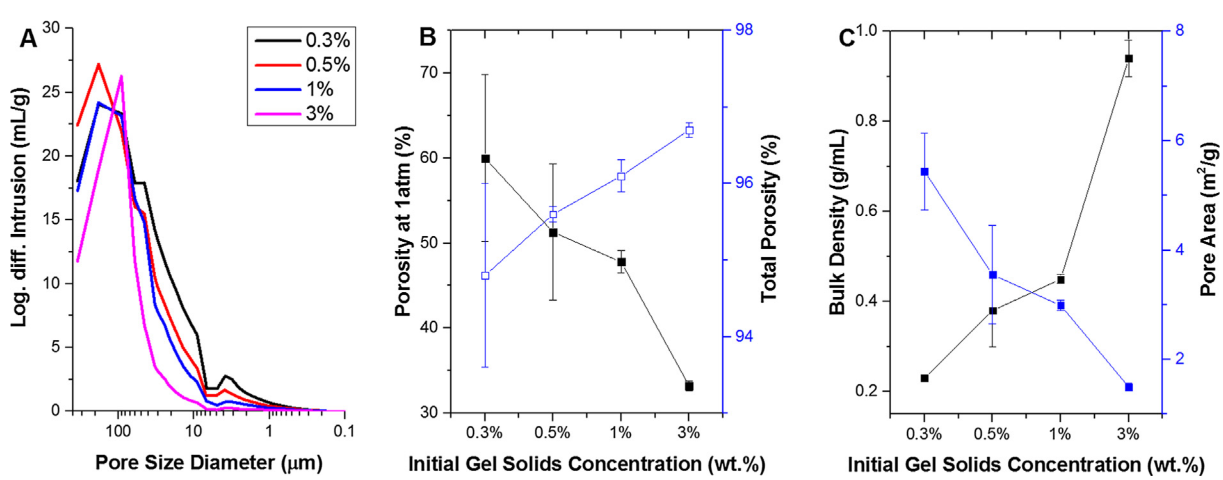


**Fig. 2.** (A) Pore size distribution of nanocellulose foams (−80 °C) at different solids concentrations. Foam properties such as (B) porosity (1 atm[a] and total[b]), (C) bulk density and pore area derived from mercury porosimetry. Further details on porosimetry data and related calculations are provided in the Supplementary Information. Notes: [a]Porosity at 1 atm is calculated by: $Porosity\ (1atm) = \left(1 - \frac{Bulk\ Density\ (1atm)}{Skeletal\ Density}\right) \times 100\%$. [b]Total porosity is calculated by: $Total\ Porosity = \left(\frac{Pore\ Volume}{Skeletal\ Volume + Pore\ Volume}\right) \times 100\%$.

### 3.2. Effect of surface charge

Fig. 3 shows the effect of the nanocellulose carboxylate group content on the foam absorption capacity. Lowering the carboxylate group from 1.2 mmol/g to 0.65 mmol/g resulted in lower absorption values for all concentrations tested.

### 3.3. Effect of freezing rate

The formation of nanocellulose foams is a two-step process which includes freezing of the nanocellulose gels and sublimation of the frozen water. In this study, the effect of freezing rate is studied by freezing at different temperatures (−20 °C, −80 °C, −196 °C). The freezing rate will be the slowest at −20 °C whereas freezing at −196 °C will be the fastest. The lyophilisation step is kept constant in this study. The effect of freezing rate on the performance of nanocellulose foams in absorbing deionised water is shown in Fig. 4A. Aside from 0.3 wt%, foams processed at −80 °C has performed slightly better than −20 °C. Freezing rate was modified to control foam morphology. Freezing at the lowest rate (−20 °C) results in sheet-like structures with interspersed pores (Fig. 4B) whereas at the fastest freezing rate (−196 °C), the pores formed are more uniform (Fig. 4D). At −80 °C, the structure formed is a combination of those from the two freezing rates (Fig. 4C).

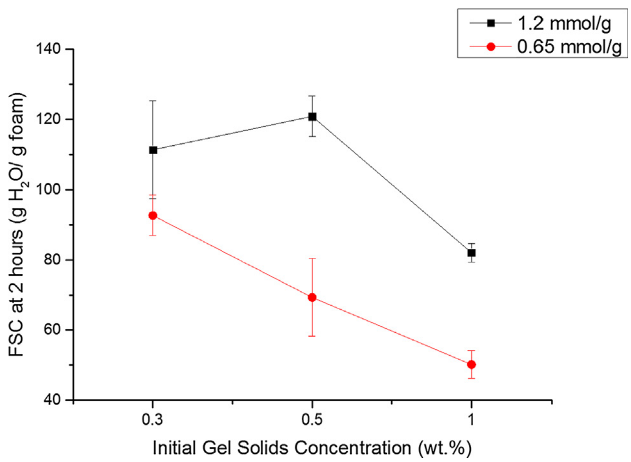


**Fig. 3.** Effect of cellulose fibre surface charge of nanocellulose foams (−80 °C) at different solids concentration on FSC in deionised water.

### 3.4. Absorption of saline

Fig. 5 shows the FSC of nanocellulose foam in 0.9 wt% saline. For all foams, lower FSC values are recorded in saline than in deionised water. Absorption after 2 h is very similar for all concentrations tested with capacity ranging between 50 g/g and 70 g/g. The saline absorption capacity of nanocellulose foams were slightly lower to those of commercial SAP (80 g/g).

## 4. Discussion

### 4.1. Effect of foam and fibre properties on superabsorbent capacity

In this study, fibre properties, including the initial solids concentration and surface charge, are varied to determine the effect on the superabsorption performance of nanocellulose gels. When the initial gel solids concentration was varied from 0.3 wt% to

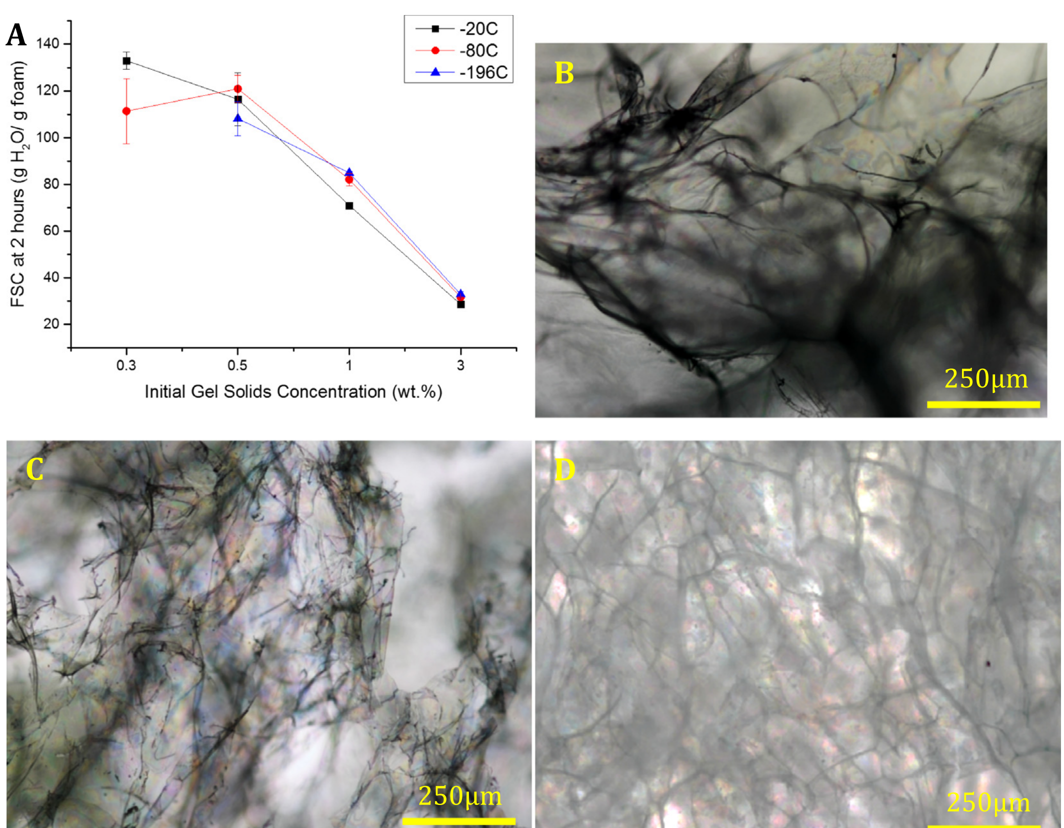


**Fig. 4.** (A) The effect of freezing rate (initial freezing at −20 °C, −80 °C, and 196 °C) on the FSC in deionised water. Optical microscopy illustrating the effect of freezing at (B) −20 °C (C) −80 °C, and (D) −196 °C on the morphology of nanocellulose foams.

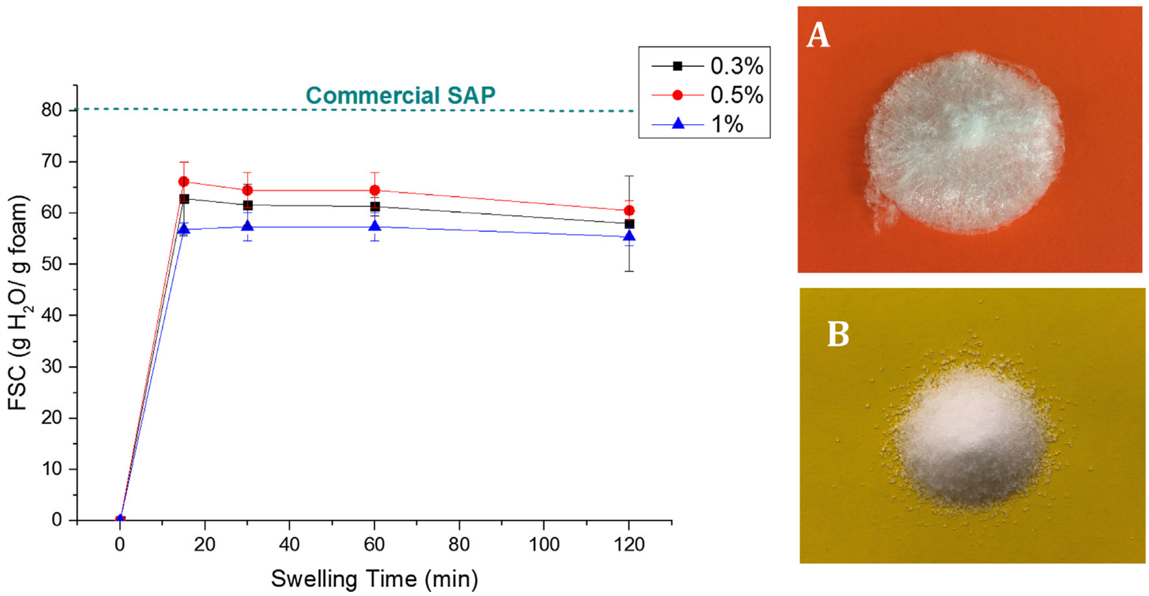


**Fig. 5.** FSC of nanocellulose (−80 °C) in 0.9 wt% saline as a function of swelling time compared against the equilibrium absorption capacity of a commercial SAP polymer. Images showing a (A) NC foam and (B) commercial SAP polymer.

0.5 wt% (−80 °C), FSC values were similar. However, further increase in the fibre concentration (0.5 wt% to 3 wt%) resulted in lower FSC values due to the limited availability of the foam internal structure because of a narrower pore distribution (Fig. 2). The percentage of accessible pores, quantified by the porosity at 1 atm, decreases with increasing initial solids concentration. For instance, increasing the fibre density by an order of magnitude (0.3 wt% to 3 wt%) resulted in halving (~50% decrease) the available pores at 1 atm. However, the high absorption capacity of nanocellulose cannot be explained merely by the available pore volume shown in Fig. 6. For instance, the foam from 0.5 wt% gel, which is capable of absorbing 120 g/g, has a calculated volume of easily accessible pores of 1.4 mL/g foam (at 1 atm) and a total pore volume of 29 mL/g foam. The available pore volume cannot solely take into account such a large absorption. This means that the 0.5 wt% foam structure needs to significantly expand by a factor four its initial volume. The absorption capacity of nanocellulose can be attributed largely to the swelling of the fibre network leading to physical entrapment of liquid water loosely held between nanofibres by capillary forces. This is in contrast to the absorption mechanism

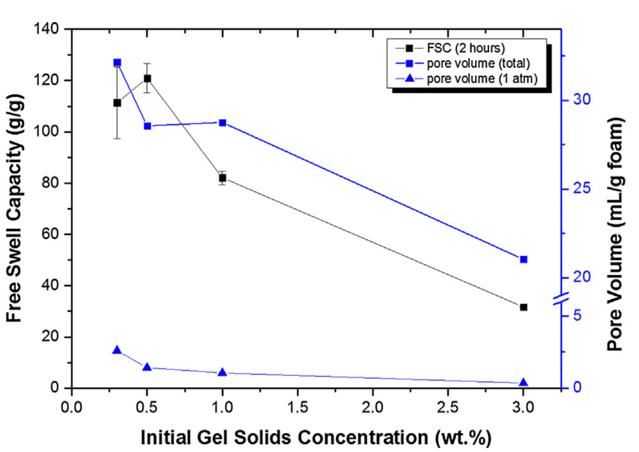


**Fig. 6.** Effect of the initial gel solids content on the superabsorbent nanocellulose foam FSC (−80 °C) in deionised water (2 h) and available pore volume at 1 atm and total pore volume from mercury porosimetry.

of conventional polyacrylic SAPs which are composed of longer polymer chains (DP = ~20,000 [36], compared to nanocellulose DP = ~600 [37]) with a higher density of COO— groups participating in hydrogen bonding with water.

Fibre surface charge is indicative of the amount of $COO^-$ groups which participate to water absorption. Fibrous structures with a higher concentration of $COO^-$ groups can be expected to have higher absorption and FSC values. Nanocellulose fibres have a theoretical and demonstrated upper carboxylate limit of 1.6 mmol/g fibre [38]. Our fibres contain 1.2 mmol $COO^-$/g fibre, indicating near-complete oxidation of the C6 hydroxyl group. Doubling the carboxylate content on the cellulose polymer resulted in an increase in the absorption capacity (19 g/g to 51 g/g), as shown in Fig. 3.

### *4.2. Swelling kinetics of nanocellulose foams*

The swelling of nanocellulose foams over time can be characterised by two distinct regimes: (a) the initial rapid uptake of absorbate and (b) the asymptotic increase of absorption towards the equilibrium absorption capacity $W_\infty$ (Fig. 1) [39]. Swelling kinetic parameters such as the equilibrium absorption capacity $W_\infty$ (g/g) and swelling rate constant $k_s$ (g/g min) describing the swelling kinetics of the foams can be estimated by assuming a second order rate of swelling of absorption $W$ (g/g) at swelling time $t$ (min) as derived by Schott [40]:

$$\frac{dW}{dt} = k_s(W_\infty - W)^2 \tag{5}$$

Eq. (5) can be linearised by setting the following conditions: $W = 0$ at $t = 0$ and $W = \mathrm{W}$ at $t = \mathrm{t}$, resulting in Eq. (4):

$$\frac{t}{W} = A + Bt \tag{6}$$

where:

$$B = \frac{1}{W_\infty} \tag{7}$$

$$A = \frac{1}{\left(\frac{dW}{dt}\right)_0} \tag{8}$$

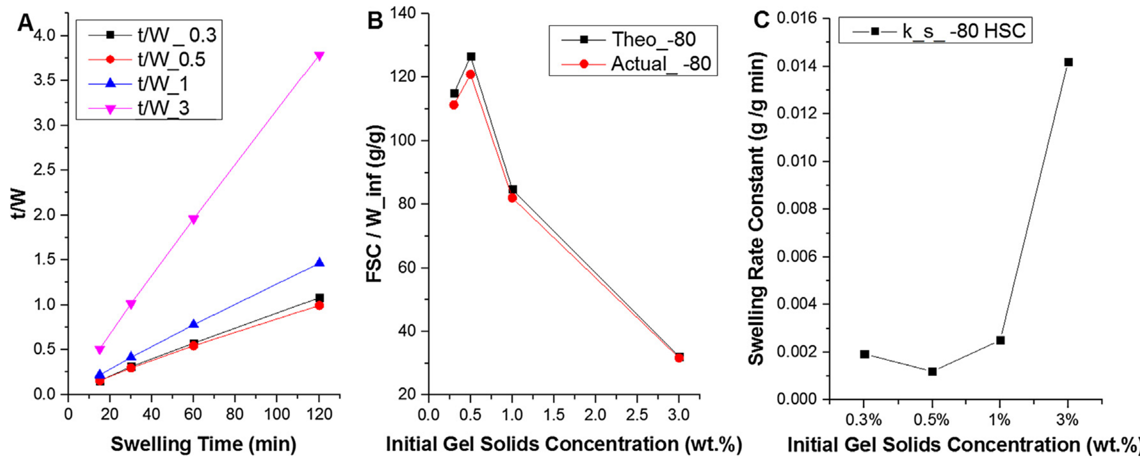


**Fig. 7.** Calculated swelling kinetic parameters of nanocellulose foams (−80 °C): (A) Linearisation of FSC by Schott's equation (B) equilibrium absorption capacity $W_\infty$ and (C) swelling rate constant.

$$k_s = \frac{1}{AW_\infty^2} \tag{9}$$

Linearising Eq. (6) by plotting *t/W versus t* provides good fit with the experiments ($R^2 > 0.99$) (Fig. 7A). This suggests that the second-order kinetic assumption with respect to capacity is indicative either of a bimolecular mechanism (water-cellulose) or of a system with diffusion constraints. The actual absorption capacity at 2 h is close to the theoretical capacity $W_\infty$, which indicates that the foams reach saturation within the testing period (Fig. 7B). In all concentrations tested, at least 90% of the theoretical capacity was reached within the first 30 min of testing – independent of the initial gel concentration. The foam swelling rate constant is constant between 0.3 wt% and 1 wt% and increased dramatically at 3 wt% (Fig. 7C). The increase in the swelling rate constant at increasing solids content can be due to saturation reached much faster because of smaller pores and numerous inaccessible carboxylate groups leading to an overall lower free swell capacity.

### 4.3. Effect of freezing rate and absorbate on superabsorbent capacity

The freezing rate of nanocellulose before lyophilisation dictates either nucleation or crystal growth of ice in the gel influencing the nanocellulose porous structure [41]. Freezing at −20 °C promotes the crystallisation of larger ice crystals as the degree of supercooling is low [41]. Hence, large pores are produced in certain regions where the ice crystals are formed, and individual fibres are aggregated forming sheet-like structures together, as seen from Fig. 4B. Freezing at a faster rate (−80 °C) led to an intermediate state wherein there are still sheets formed with the hornified fibres producing a more uniform structure. Vitrification of the network structure is promoted by freezing at a much faster rate (−196 °C) producing a more homogeneous pore structure. This is due to the fibre spacing present within the gel structure (electrostatic repulsion) being maintained upon foam formation. In this instance, the higher rate of freezing promoted the rapid nucleation of smaller ice crystals leading to a more homogenous pore structure [42]. The foams produced at −196 °C however were brittle and difficult to handle in contrast to those treated at −20 °C and −80 °C. Other studies have corroborated with our findings and also reported brittle foams produced from freezing in liquid nitrogen [30,43]. Hence, it was rather difficult to test low solids content foams such as 0.3 wt%; these results were omitted from Fig. 4A. Although, the morphologies of nanocellulose structures are visibly affected by the freezing rate, the absorption capacity remains similar. This could be due to the hornified fibres in foams prepared at −20 °C and −80 °C that separate partially while swelling.

The lower values of absorption in saline compared to deionised water is due to the charge shielding from the ions. This reduces the interaction with the $COO^-$ groups and the water molecules. The saline capacity of the nanocellulose foams is similar to those reported by Theliander et al. with FSCs ranging between 30 and 60 g/g [26–29]. The performance of the nanocellulose foams is slightly lower in contrast to a granulated commercial polyacrylic acid SAP. Further optimising the method to produce the foams may yield similar performance to commercial SAPs.

## 5. Conclusion

Cellulose-based superabsorbents were investigated as sustainable substitutes for the current acrylic acid and acrylamide-based SAPs. While numerous studies have examined cellulose-based superabsorbents using various methodologies, few have analysed the SAP structure-performance relationship of TEMPO-oxidised nanocellulose foams [26–29,44]. In particular, the effect of fibre content and processing conditions (ie. freezing conditions) were not investigated. Moreover, the kinetics and mechanism of absorption for nanocellulose have not been studied. TEMPO-mediated oxidation produces charged nanocellulose fibres capable of forming cellulosic colloidal gels. The carboxylate groups of TEMPO-oxidised nanocellulose can be exploited for superabsorption. In this study, the potential of TEMPO-oxidised fibres as a superabsorbent polymer is demonstrated. The effect of fibre properties and processing conditions on the resulting nanocellulose foam morphology and its superabsorption performance is determined. Nanocellulose foam density is dictated by the initial gel solids concentration. The best performing foams are at 0.3–0.5 wt% frozen at −80 °C which are capable of absorbing 110–120 g/g $H_2O$. In general, a higher solids concentration produces foams with a narrower pore size distribution and a lower porosity leading to a decreased absorption performance. Nanocellulose foams follow a pseudo-second order absorption kinetics which is affected by foam density. Freezing temperature affects the foam network structure by dictating whether ice nucleation or crystallisation dominates, expanding or not the fibrous structure. A homogeneous porous structure is formed at the fastest freezing rate (−196 °C) whereas uneven sheet-like formations were observed at lower freezing rates (−20 °C, −80 °C). The free swell capacity remained unaffected even with differences in morphology. Changing the absorbate from deionised water to 0.9 wt% NaCl, mimicking bodily fluids, resulted in the decrease of free swell capacity (FSC) values due to charge shielding. However, the nanocellulose foam performance in saline is already comparable with granulated polyacrylamide SAPs which have been optimised over the last 3 decades. With the results already achieved, the clear link between process-structure-properties and a robust optimization methodology, matching the properties of the current commercial polyacrylic superabsorbent polymers has become a realistic target for cellulose composites. Absorption behaviour in saline can be further improved by blending nanocellulose with biopolymers and optimising the shape and microstructure of foams. Nanocellulose foams has emerged as a high performance, renewable and biodegradable superabsorbent material for biomedical, personal care and environmental applications.

## Acknowledgments

This work was funded by the ARC Bioprocessing Advance Manufacturing Industry Research Transformation (BAMI) Hub IH13100016, Visy, Norske Skog, Orora, Oji Fibre Solutions, Australian Paper and Circa. Special thanks to Anthony De Girolamo (Monash University) for running the porosimetry experiments.

## Appendix A. Supplementary material

Supplementary data to this article can be found online at https://doi.org/10.1016/j.jcis.2018.11.112.

## References

[1] J.R. Gross, in: Studies in Polymer Science, Elsevier, 1990, p. 3.
[2] H. Omidian, S.A. Hashemi, P.G. Sammes, I. Meldrum, Polymer 39 (1998) 6697.
[3] H. Warson, Modern Superabsorbent Polymer Technology, Wiley-VCH, New York, 2000.
[4] P. Chen, W.A. Zhang, W. Luo, Y.e. Fang, J. Appl. Polym. Sci. 93 (2004) 1748.
[5] J.V. Rogers, W.R. Richter, Y.W. Choi, A.K. Judd, Lett. Appl. Microbiol. 48 (2009) 180.
[6] C. Wiegand, M. Abel, P. Ruth, U.C. Hipler, J. Mater. Sci.: Mater. Med. 22 (2011) 2583.
[7] N. Lavoine, L. Bergström, J. Mater. Chem. A 5 (2017) 16105.
[8] H. Ferfera-Harrar, N. Aouaz, N. Dairi, Polym. Bull. 73 (2016) 815.
[9] M. Dalaran, S. Emik, G. Güçlü, T.B. İyim, S. Özgümüş, Desalination 279 (2011) 170.
[10] L. Serna-Cock, M.A. Guancha-Chalapud, Acta Agronómica 66 (2017) 495.
[11] X. Xu, B. Bai, C. Ding, H. Wang, Y. Suo, Ind. Eng. Chem. Res. 54 (2015) 3268.
[12] M.A. Hubbe, A. Ayoub, J. Daystar, R. Venditti, J. Pawlak, in: (Ed.)^(Eds.) BioResources, 2013, p 6556.
[13] R. Gavillon, T. Budtova, Biomacromolecules 9 (2008) 269.
[14] R. Sescousse, R. Gavillon, T. Budtova, Carbohydr. Polym. 83 (2011) 1766.
[15] S.R. Djafari Petroudy, J. Ranjbar, E. Rasooly Garmaroody, Carbohydr. Polym. 197 (2018) 565.
[16] A. Olad, H. Zebhi, D. Salari, A. Mirmohseni, A. Reyhani Tabar, Mater. Sci. Eng.: C 90 (2018) 333.
[17] A. Olad, H. Zebhi, D. Salari, A. Mirmohseni, A. Reyhanitabar, J. Porous Mater. 25 (2018) 1325.
[18] A.I. Raafat, M. Eid, M.B. El-Arnaouty, Nucl. Instrum. Methods Phys. Res., Sect. B 283 (2012) 71.
[19] Z. Wang, A. Ning, P. Xie, G. Gao, L. Xie, X. Li, A. Song, Carbohydr. Polym. 157 (2017) 48.
[20] A. Adair, A. Kaesaman, P. Klinpituksa, Polym. Test. 64 (2017) 321.
[21] T. Fekete, J. Borsa, E. Takács, L. Wojnárovits, Carbohydr. Polym. 166 (2017) 300.
[22] H. Kono, S. Fujita, Carbohydr. Polym. 87 (2012) 2582.
[23] H. Dai, H. Huang, J. Agric. Food. Chem. 65 (2017) 565.
[24] L.-Y. Long, Y.-X. Weng, Y.-Z. Wang, Polymers 10 (2018) 623.
[25] T. Saito, S. Kimura, Y. Nishiyama, A. Isogai, Biomacromolecules 8 (2007) 2485.
[26] P.W. Brodin, H. Theliander, BioResources 7 (2012) 1666.
[27] F.W. Brodin, H. Theliander, Cellulose 20 (2013) 1.
[28] F.W. Brodin, Y. Sonavane, H. Theliander, BioResources 8 (2013) 2099.
[29] F.W. Brodin, K. Lund, H. Brelid, H. Theliander, Cellulose 19 (2012) 1413.
[30] F. Jiang, Y.-L. Hsieh, J. Mater. Chem. A 2 (2014) 350.
[31] F. Jiang, Y.-L. Hsieh, J. Mater. Chem. A 2 (2014) 6337.
[32] F. Jiang, Y.-L. Hsieh, ACS Sustain. Chem. Eng. 4 (2016) 1041.
[33] L. Mendoza, T. Gunawardhana, W. Batchelor, G. Garnier, J. Colloid Interface Sci. 525 (2018) 119.
[34] L. Mendoza, W. Batchelor, R.F. Tabor, G. Garnier, J. Colloid Interface Sci. 509 (2018) 39.
[35] D. da Silva Perez, S. Montanari, M.R. Vignon, Biomacromolecules 4 (2003) 1417.
[36] H. Fujita, K. Mitsuhashi, T. Homma, J. Colloid Sci. 9 (1954) 466.
[37] A. Isogai, T. Saito, H. Fukuzumi, Nanoscale 3 (2011) 71.
[38] Y. Okita, T. Saito, A. Isogai, Biomacromolecules 11 (2010) 1696.
[39] X. Shi, W. Wang, A. Wang, Carbohydr. Polym. 94 (2013) 449.
[40] H. Schott, J. Macromol. Sci., Part B 31 (1992) 1.
[41] W.L. Li, K. Lu, J.Y. Walz, Int. Mater. Rev. 57 (2012) 37.
[42] F. Martoïa, T. Cochereau, P.J.J. Dumont, L. Orgéas, M. Terrien, M.N. Belgacem, Mater. Des. 104 (2016) 376.
[43] J. Erlandsson, T. Pettersson, T. Ingverud, H. Granberg, P.A. Larsson, M. Malkoch, L. Wågberg, J. Mater. Chem. A 6 (2018) 19371.
[44] J. Ma, X. Li, Y. Bao, RSC Adv. 5 (2015) 59745.